Supporting information for

A high performance and low cost poly(dibenzothiophene-S,S-dioxide)@TiO_2 composite with hydrogen evolution rate up to 51.5 mmol h^{-1} g^{-1}

Ge Shu,[a] Ye Wang,[b] Yuda Li,[a] Song Zhang,*[b] Jia-Xing Jiang[c] and Feng Wang*[a]

[a]Key Laboratory for Green Chemical Process of Ministry of Education, School of Chemical Engineering and Pharmacy, Wuhan Institute of Technology, Wuhan 430205, P. R. China. E-mail: psfwang@wit.edu.cn

[b]State Key Laboratory of Magnetic Resonance and Atomic and Molecular Physics, Innovation Academy for Precision Measurement Science and Technology, Chinese Academy of Sciences, Wuhan 430071, P. R. China, University of Chinese Academy of Sciences, Beijing 100049, P. R. China, E-mail: zhangsong@wipm.ac.cn

[c]Key Laboratory for Macromolecular Science of Shaanxi Province, Shaanxi Key Laboratory for Advanced Energy Devices, School of Materials Science and Engineering, Shaanxi Normal University, Xi'an, 710062, P. R. China

Characterization

The Fourier transform infrared (FT-IR) spectroscopy was collected on KBr disks using a Tensor 27 spectrometer in transmission mode. The structural order of samples was tested by Powder X-ray diffraction (PXRD, DX-2700). Field-emission scanning electron microscopy (SEM, JSM-7001F) and high-resolution transmission electron microscopy (TEM, H-7650) were employed to observe the nanomorphology of samples. The binding energies determined by XPS (Bruker, D8 Advance) were

corrected by reference to the adventitious carbon peak (284.8 eV) for each sample. The energy dispersive spectroscopy (EDS) was obtained on an Apollo XLT SDD detector. The content of Pd in sample was measured by ICP-OES/MS (Agilent 720ES). The UV-vis diffuse reflectance spectra (DRS) of was recorded by a UV-vis spectrophotometer (UV-Lambda 950). Photoluminescence (PL) spectra were measured under excitation wavelength at 420 nm (Shimadzu F-7000 PC). Time-resolved PL spectra were obtained on an Edinburgh Instruments FLS 980 fluorescence spectrometer. Electrochemical impedance spectroscopy (EIS) measurements were carried out using a standard three-electrode cell system.

Time-Resolved Transient Absorption Measurements

The femtosecond resolved transient absorption measurements are based on a regeneratively amplified femtosecond laser system. The detailed description of the femtosecond laser system has already been published.[1,2] Here some important features of the setup will be described in brief. The seed beam is generated by a commercial Ti:sapphire oscillator and amplified by a Nd:YLF pumped regenerative amplifier to produce the fundamental pulse. The fundamental pulse is centered at 800 nm with a repetition rate of 1 kHz, 35 fs pulse width and energy up to 1mJ/pulse. The 400 nm excitation pulses were obtained by the second harmonic generation in a 0.5 mm BBO crystal and were subsequently attenuated to be ~ 2 μJ/pulse. A small portion of the fundamental pulses passed through an optical delay line and were focused into a 1 mm CaF_2 plate to generate a white continuum 450-700 nm. In order to eliminate the effect of the background and improve the measuring sensitivity, the white light was

split into the probe and the reference beams by being reflected from the front and back surfaces of a quartz plate. All the measurements were carried out under magic angle (54.7°) to avoid the rotational decay processes and effect of polarization. To minimize interference by the photoproducts formed during the experiments, the sample was put into a flow cell, which includes 0.2 mm quartz windows. The pump and probe pulses were spatially overlapped in the sample with an intersection angle of < 4° and the reference pulses passed through the sample at a different spot. Finally, all the pulses were collected in a CCD camera (PI-MAX, 1024×256 pixel array) equipped with a spectrometer (Princeton, SpectraPro 2500i) and the final transient absorption spectra were detected. To obtain the cross correlation between the pump and probe pulses which determined the instrumental response function of the system and precise the zero time-delay at every probe wavelength, the optical Kerr-gate experiments were carried out. The cross correlation in our measurements is about 250 fs.

Apparent quantum yield (AQY) measurement

The AQY measurement for the photocatalytic experiment was carried out using monochromatic Xe lamp with band pass filter. The light intensities at 420, 450, and 500 nm are 26, 32, 30 mW cm^{-2}, respectively. During the photocatalysis, PDBTSO@TiO_2 (10 mg) nanocomposite was suspended in 100 mL aqueous solution in the presence of TEOA (20 vol%) and hexachloroplatinic acid (3 wt %). The AQY was calculated based on following equation:

$$AQY\ (\%) = \frac{2 \times Number\ of\ evolved\ H_2\ molecules}{Number\ of\ incident\ photons} \times 100\%$$

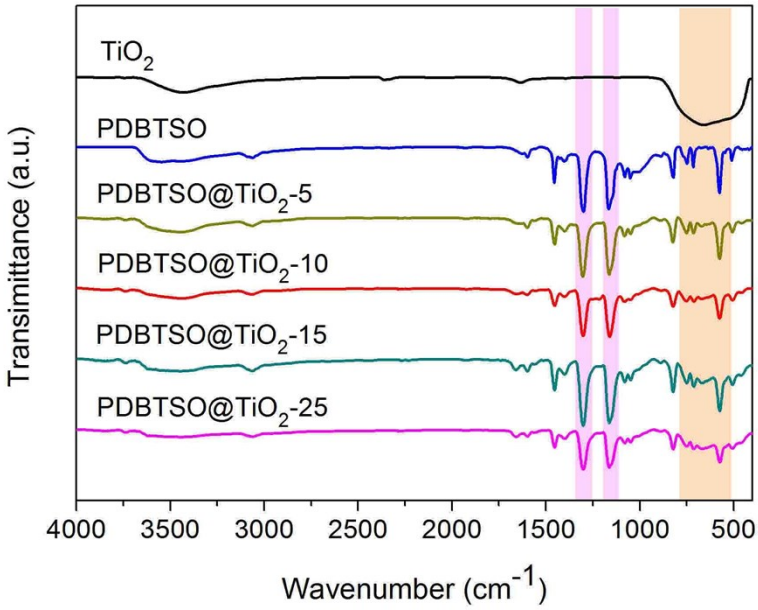

Figure S1. FTIR spectra of TiO_2, PDBTSO and PDBTSO@TiO_2.

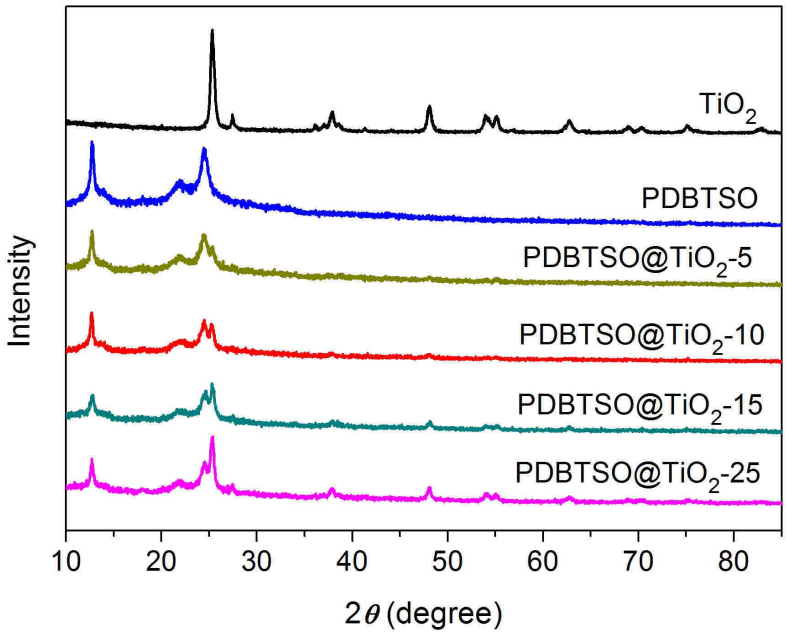

Figure S2. PXRD patterns of TiO_2, PDBTSO and PDBTSO@TiO_2.

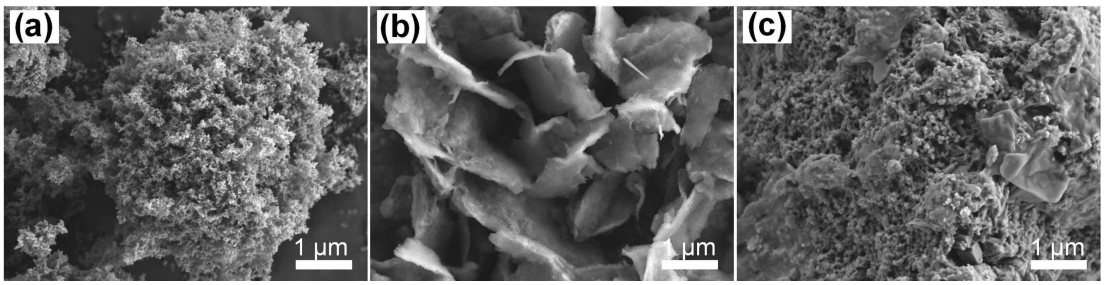

Figure S3. SEM images of TiO_2, PDBTSO and PDBTSO@TiO_2-10.

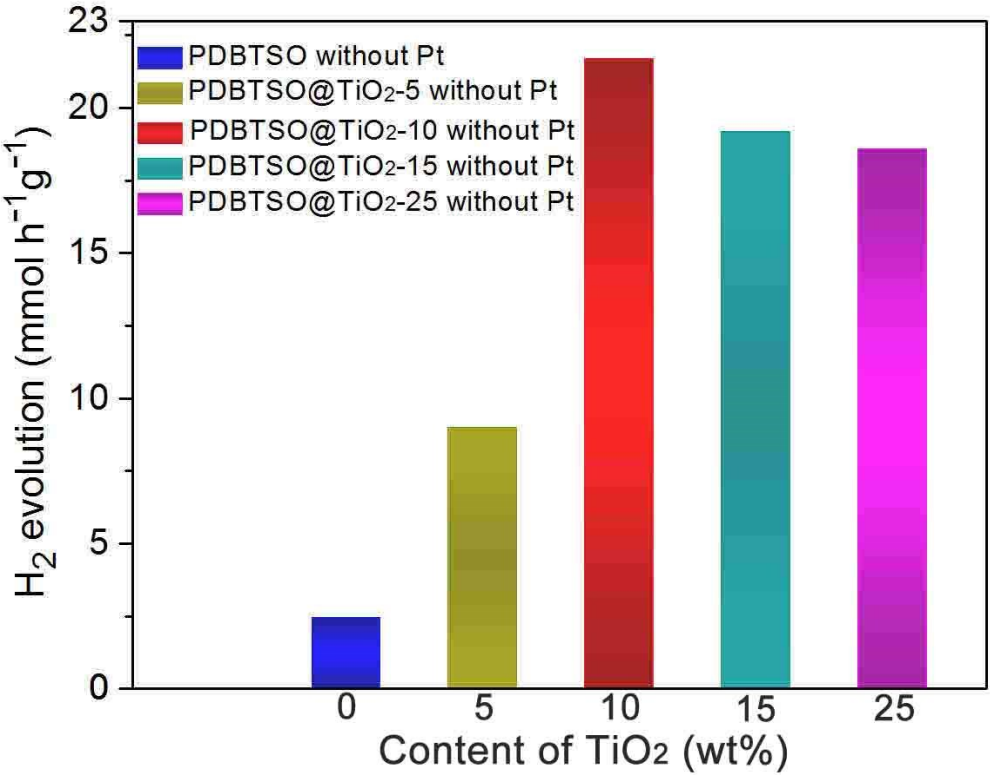

Figure S4. Effect of TiO_2 loading amount on the hydrogen production activity over PDBTSO@TiO_2 without Pt co-catalyst. Conditions: 10 mg sample, 100 mL 20 vol% TEOA/H_2O, visible light irradiation.

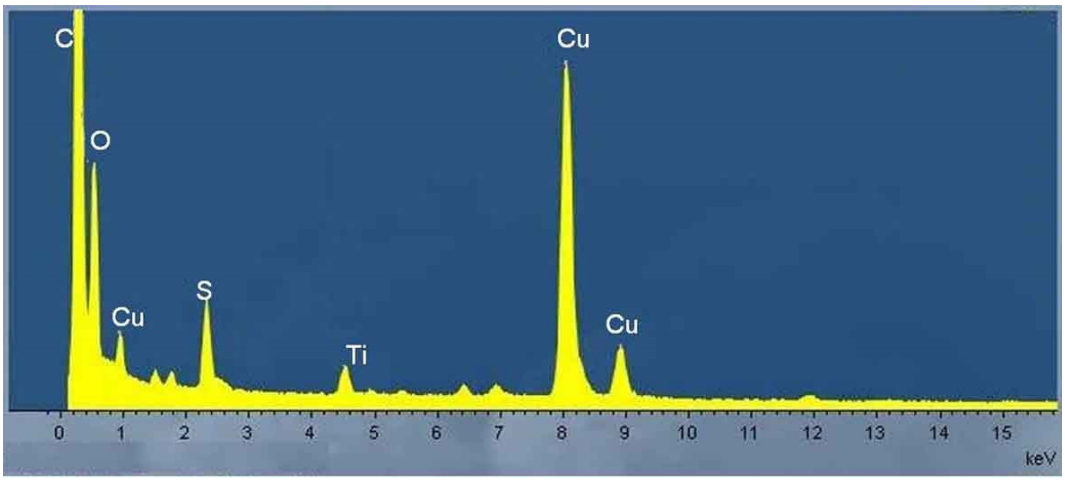

Figure S5. EDS spectra of PDBTSO@TiO_2-10, the signal of Cu is from the substrate of quartz.

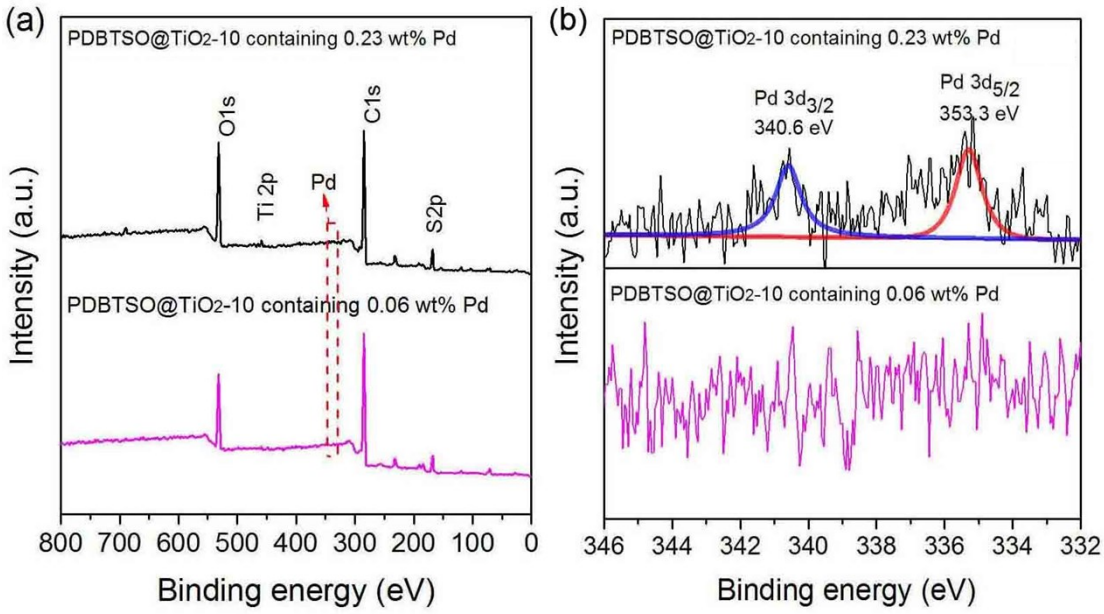

Figure S6. XPS spectra of PDBTSO@TiO_2-10, (a) Survey spectra, (b) Pd 3d.

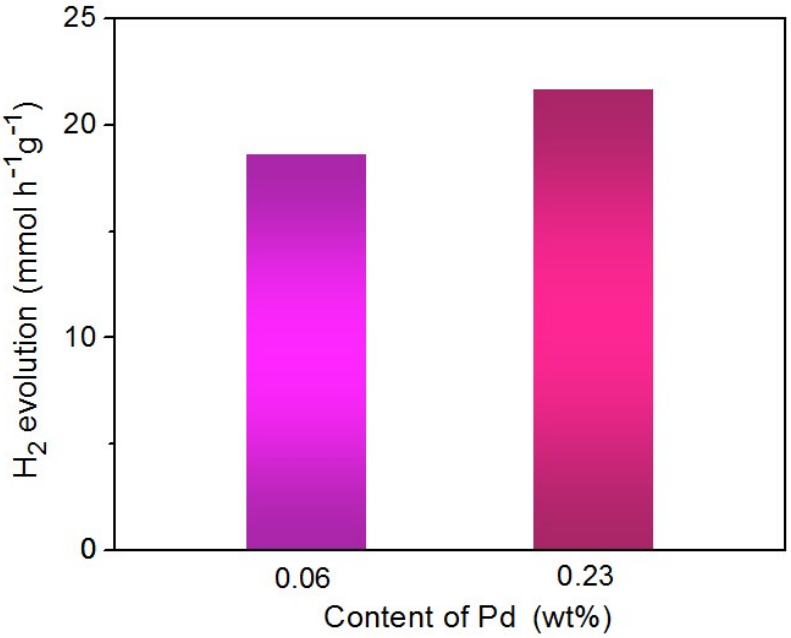

Figure S7. Compared HER of PDBTSO@TiO_2-10 composites containing varied amounts of residual Pd as determined by ICP-OES.

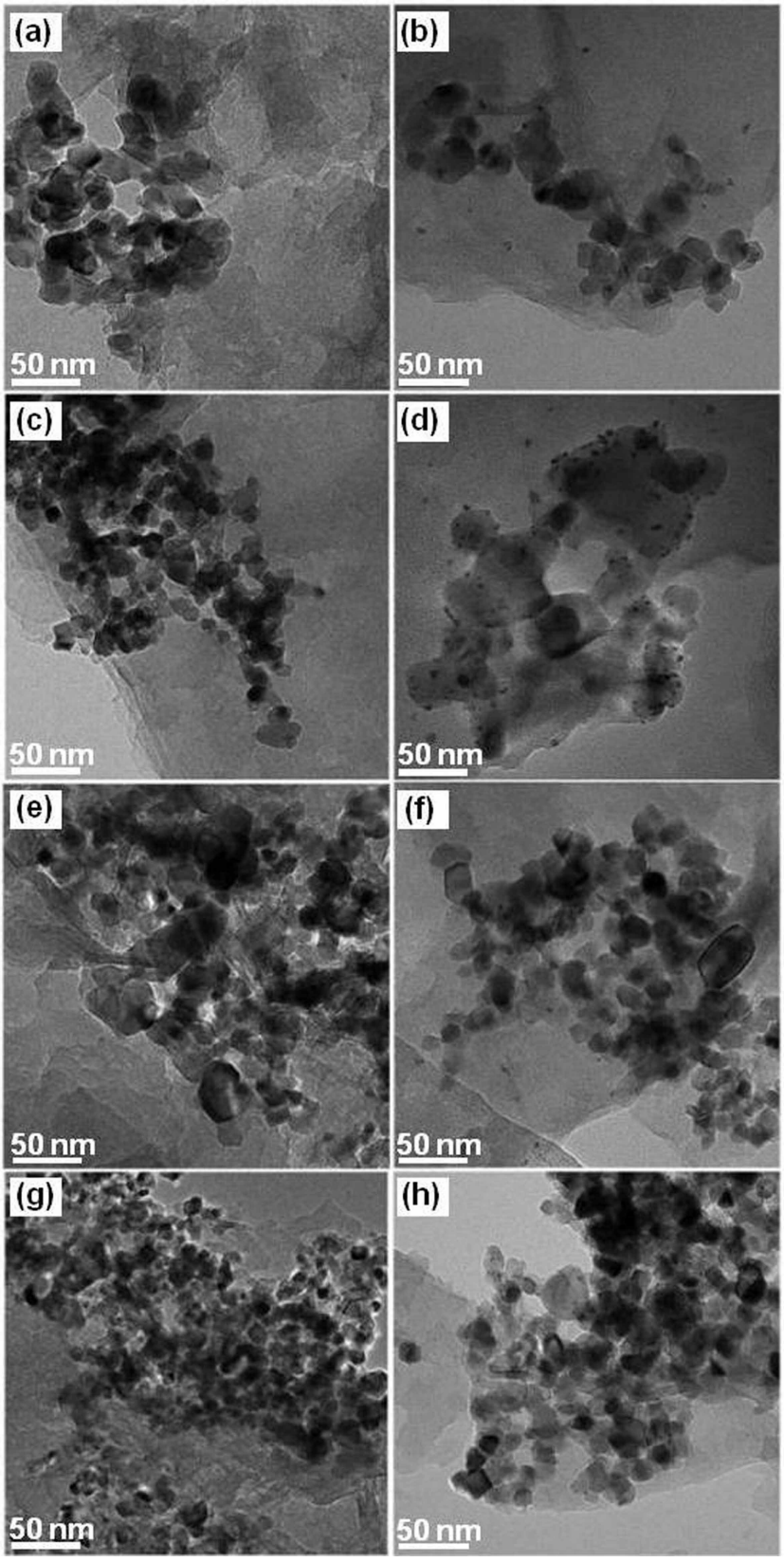

Figure S8. TEM images of (a) PDBTSO@TiO_2-5, (c) PDBTSO@TiO_2-10, (e) PDBTSO@TiO_2-15, and (g) PDBTSO@TiO_2-25 before in-situ photodeposition of Pt, and (b) PDBTSO@TiO_2-5, (d) PDBTSO@TiO_2-10, (f) PDBTSO@TiO_2-15, and (h)

PDBTSO@TiO_2-25 after in-situ photodeposition of Pt.

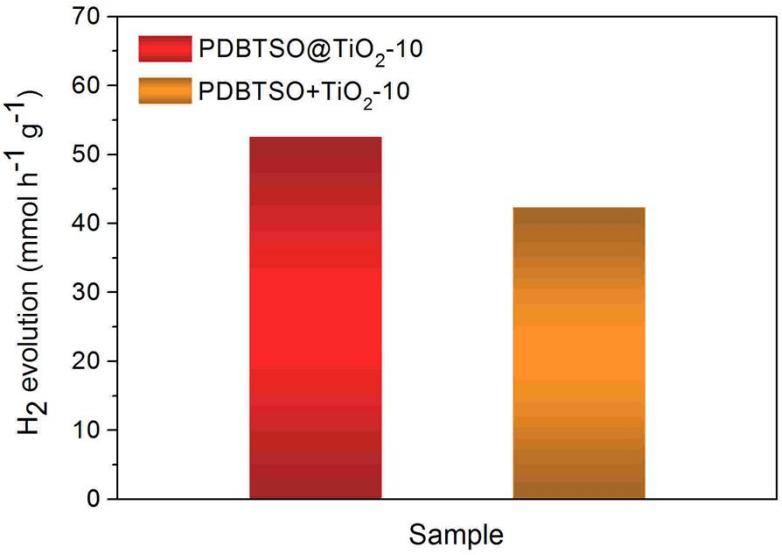

Figure S9. HER of PDBTSO@TiO_2-10 nanocomposite and the physically blended sample PDBTSO+TiO_2-10 with same phase composition. Experimental conditions: 10 mg sample; 3 wt% Pt co-catalyst; visible light irradiation.

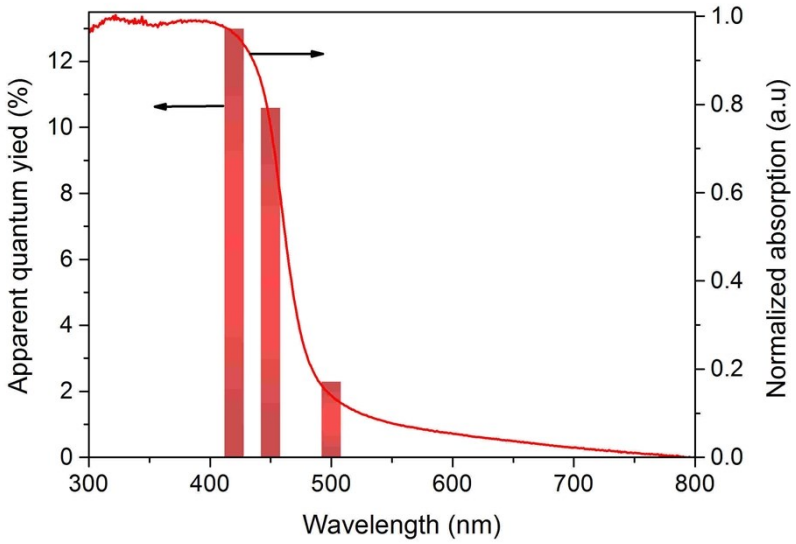

Figure S10. Wavelength dependence of AQY on hydrogen production and UV-vis absorption spectra of PDBTSO@TiO_2-10.

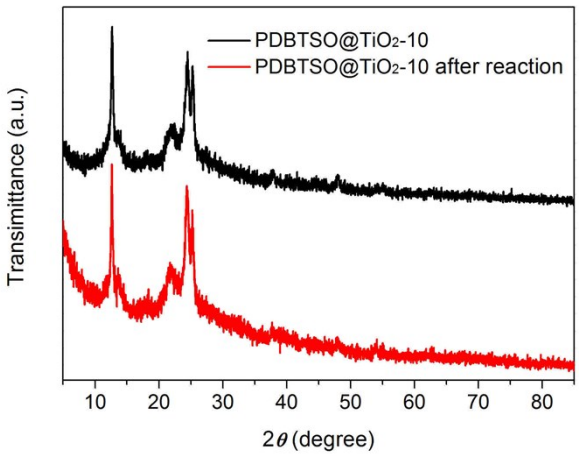

Figure S11. XRD patterns of PDBTSO@TiO_2-10 before and after the photocatalytic reaction.

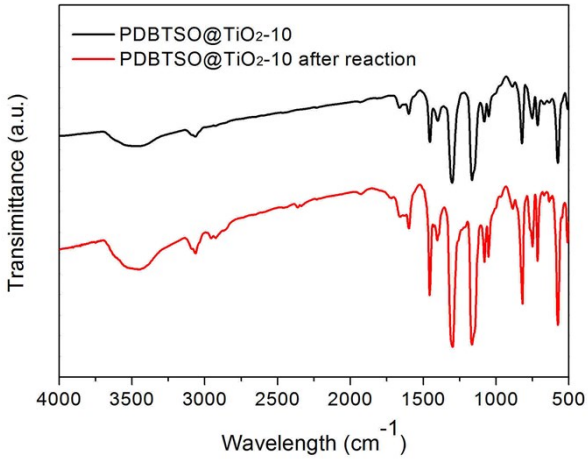

Figure S12. FTIR spectra of PDBTSO@TiO_2-10 before and after the photocatalytic reaction.

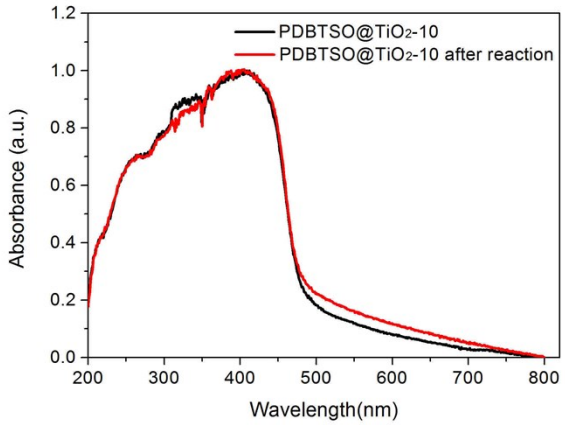

Figure S13. UV-vis absorption spectra for PDBTSO@TiO_2-10 before and after the photocatalytic reaction.

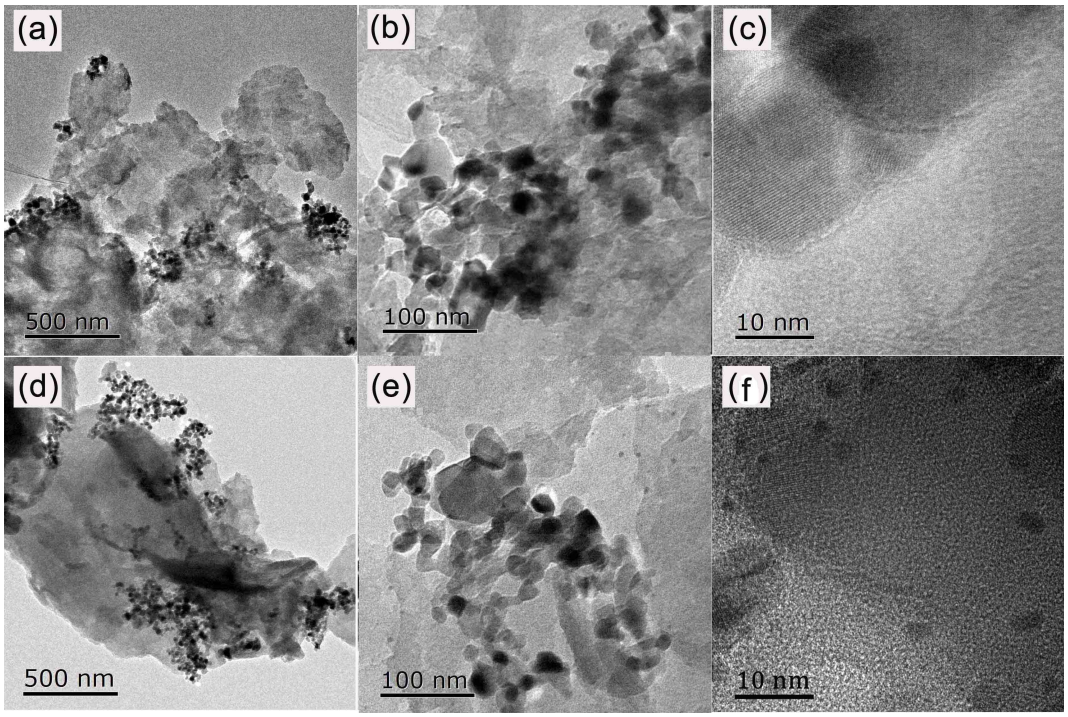

Figure S14. TEM (a, b, d, e) and HRTEM (c, f) images of PDBTSO@TiO_2-10 (a, b, c) before in-situ photodeposition of Pt and PDBTSO@TiO_2-10 (d, e, f) after in-situ photodeposition of Pt.

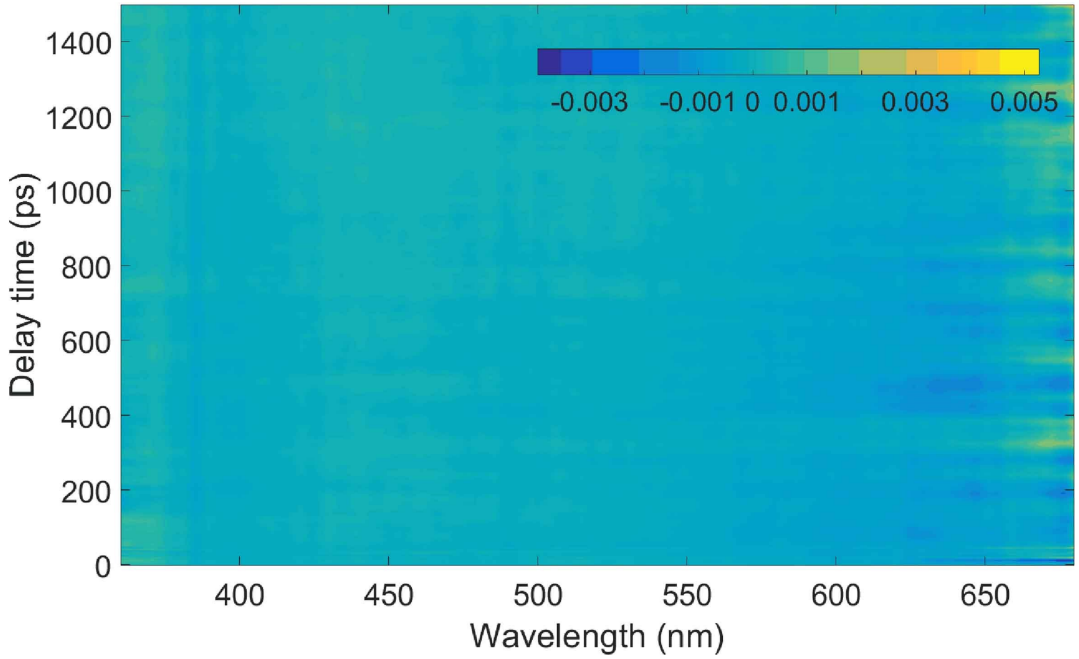

Figure S15. Two–dimensional transient absorption spectra of raw TiO_2 .with delay time up to 1400 ps. Experimental conditions: aqueous solution containing 20 vol% TEOA; 400 nm laser irradiation.

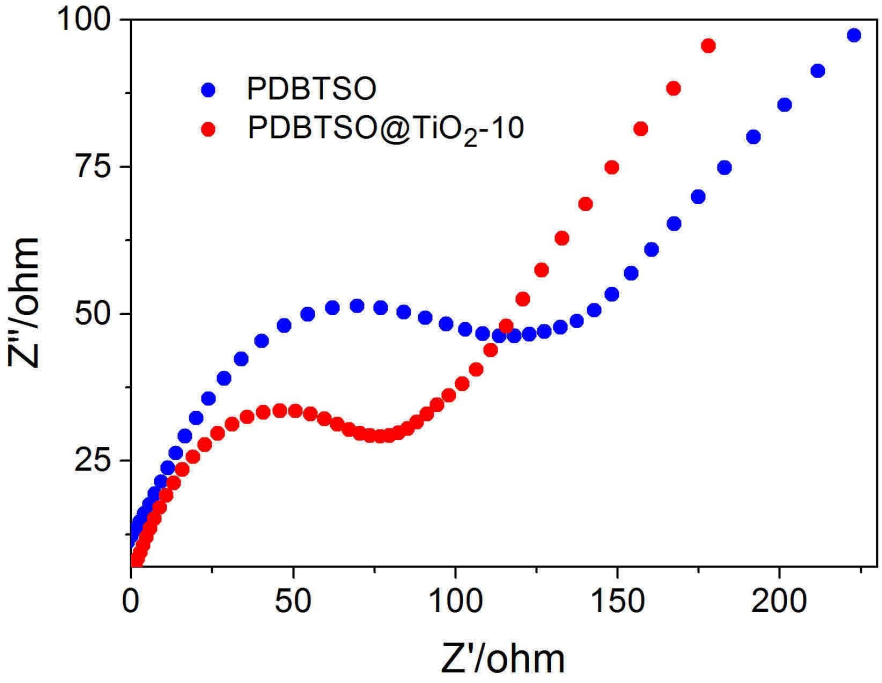

Figure S16. EIS of PDBTSO and PDBTSO@TiO_2-10.

Table S1. Comparison of representative polymer-based composite photocatalysts with ultrahigh HER activity (HER > 10 mmol h^{-1} g^{-1})

Photocatalysts	Cocatalysts	Photocatalysts mass (mg)	Light source	HER ($mmolh^{-1}$ g^{-1})	Ref.
PDBTSO/TiO_2	Pt (3 wt%)	10	λ > 420 nm	51.5	This work
$CZ_{0.5}S$@50ZS-3N/8CN	Ni_2P and g-C_3N_4	10	λ > 420 nm	55.43	S3
CNS–COF	Pt (3 wt%)	10	λ > 420 nm	46.4	S4
TxPP1@T-10	Pt (1 wt%)	100	UV-Vis	21.945	S5
S5@Pt/TiO_2	Pt	20	λ > 420 nm	21.5	S6
Ni_2P-SNO/CdS-D	Ni_2P (1 wt%)	30	λ > 420 nm	11.992	S7
NZIS-3	-	20	λ > 420 nm	11.086	S8
TiO_2-TpPa-1-COF	Pt (3 wt%)	10	λ > 420 nm	11.19	S9
CdS-CTF-1	Pt (1 wt%)	20	λ ≥ 420 nm	11.43	S10
3D CCNS	Pt (3 wt%)	10	UV-vis	27.035	S11
Ni_2P/Ni@C/g-C_3N_4-550	Ni_2P/Ni	10	λ ≥ 420 nm	18.04	S12
g-C_3N_4/C@Ni_3S_4/Ni_2P-30	Ni_3S_4/Ni_2P	10	λ ≥ 420 nm	14.49	S13
g-C_3N_4/Fe_2O_3@FeP-60	Fe_2O_3@FeP	10	λ ≥ 420 nm	12.03	S14
BE–Au–TiO_2	Au (1wt%)	30	λ ≥ 420 nm	26.04	S15
g-C_3N_4/TiO_2/rGO	rGO (1 wt%)	5	UV-Vis	23.143	S16
NiS/g-C_3N_4	NiS (0.76 wt%)	5	AM 1.5 G	16.4	S17
P3/CN	-	50	λ ≥ 420 nm	13	S18
PY-2/g-C_3N_4/Pt	Pt (1 wt%)	80	λ ≥ 420 nm	11.885	S19
NZCN30	-	5	UV-Vis	18.836	S20
α-Fe_2O_3/g-C_3N_4	Pt (3 wt%)	10	λ ≥ 420 nm	31.4	S21
TiO_2@COP64	Pt (3 wt%)	20	UV-vis	15.02	S22

1 wt% catechol-TiO_2	-	30	Solar light	10.925	S23

Table S2. Fitted decay time of PDBTSO and PDBTSO@TiO_2-10.

Sample	τ_1 (ns)	Rel(%)	τ_2 (ns)	Rel(%)	τ(ns)
PDBTSO	0.4795	58.56	2.479	41.44	1.308
PDBTSO@TiO_2-10	0.5735	50.95	2.778	49.05	1.654

References

1 S. Zhang, S. M. Sun, M. M. Zhou, L. Wang and B. Zhang, *Sci. Rep.* 2017, *7*, 43419.

2 K. Wu, T. Zhang, Z. Wang, L. Wang, L. Zhan, S. Gong, C. Zhong, Z. Lu, S. Zhang and C. Yang, *J. Am. Chem. Soc.* 2018, ***140***, 8877−8886.

3 X. W. Ma, Q. Q. Ruan, J. K. Wu, Y. Zuo, X. P. Pu, H. F. Lin, X. J. Yi, Y. Y. Li and L. Wang, *Dalton Trans.*, 2020, **49**, 6259−6269.

4 M. L. Luo, Q. Yang, W. B. Yang, J. H. Wang, F. F. He, K. W. Liu, H. M. Cao and H. J. Yan, *Small*, 2020, **16**, 2001100.

5 A. Valverde-Gonzáez, C. G. Lopez Calixto, M. Barawi, M. Gomez-Mendoza, V. A. de la Peña O'Shea, M. Liras, B. Gómez-Lor and M. Iglesias, *ACS Appl. Energy Mater.*, 2020, **3**, 4411–4420.

6 H. R. Ding, M. Y. Xu, S. C. Zhang, F. T. Yu, K. Y. Kong, Z. J. Shen and J. L. Hua, *Renew. Energ.*, 2020, **155**, 1051–1059.

7 T. P. Hu, K. Dai, J. F. Zhang and S. F. Chen, *Appl. Catal., B*, 2020, **269**, 118844.

8 C. Du, B. Yan, Z. Y. Lin and G. W. Yang, *J. Mater. Chem. A*, 2020, **8**, 207 –217.

9 C. C. Li, M. Y. Gao, X. J. Sun, H. L. Tang, H. Dong and F. M. Zhang, *Appl. Catal., B*, 2020, **266**, 118586.

10 D. K. Wang, H. Zeng, X. Xiong, M-F. Wu, M. R. Xia, M. L. Xie, J-P. Zou and S-L. Luo. *Sci. Bull.*, 2020, **65**, 113–122.

11 H. H. Gao, R. Y. Cao, S. W. Zhang, H. C. Yang and X. J. Xu, *ACS Appl. Mater. Inter.*, 2019, **11**, 2050–2059.

12 J. X. Xu, Y. H. Qi and L. Wang, *Appl. Catal., B*, 2019, **246**, 72 –81.

13 Y. H. Qi, J. X. Xu, M. J. Zhang, H. F. Lin and L. Wang, *Int. J. Hydrogen Energ*., 2019, **44**, 16336 –16347.

14 Y. H. Qi, J. X. Xu, Y. L. Fu, C. Wang and L. Wang, *ChemCatChem*, 2019, **11**, 3465–3473.

15 J. Xiao, Y. Z. Luo, Z. X. Yang, Y. G. Xiang, X. H. Zhang and H. Chen, *Catal. Sci. Technol*., 2018, **8**, 2477–2487.

16 H. Y. Hafeez, S. K. Lakhera, S. Bellamkonda, G. R. Rao, M. V. Shankar, D. W. Bahnemann and B. Neppolian, *Int. J. Hydrogen Energ*., 2018, **43**, 3892–3904.

17 H. Zhao, H. Z. Zhang, G. W. Cui, Y. M. Dong, G. L. Wang, P. P. Jiang, X. M. Wu and N. Zhao, *Appl. Catal., B*, 2018, **225**, 284–292.

18 F. T. Yu, Z. Q. Wang, S. C. Zhang, H. N. Ye, K. Y. Kong, X. Q. Gong, J. L. Hua and H. Tian, *Adv. Funct. Mater*., 2018, **28**, 1804512.

19 F. T. Yu, Z. Q. Wang, S. C. Zhang, K. Yun, H. N Ye, X. Q. Gong, J. L. Hua and H. Tian, *Appl. Catal.*, *B*, 2018, **237**, 32–42.

20 S. Kumar, N. L. Reddy, A. Kumar, M. V. Shankar and V. Krishnan, *Int. J. Hydrogen Energ*., 2018, **43**, 3988–4002.

21 X. J. She, J. J. Wu, H. Xu, J. Zhong, Y. Wang, Y. H. Song, K. Q. Nie, Y. Liu, Y. C. Yang, M-T. F. Rodrigues, R. Vajtai, J. Lou, D. L. Du, H. M. Li and P. M. Ajayan, *Adv. Energy Mater*., 2017, **7**, 1700025.

22 Q. Q. Yang, P. Peng and Z.H. Xiang, *Chem. Eng. Sci.,* 2017, **162**, 33–40.

23 P. Karthik, R. Vinoth, P. Selvam, E. Balaraman, M. Navaneethan, Y. Hayakawa and B. Neppolian, *J. Mater. Chem. A,* 2017, **5**,384–396.